SANDIA REPORT
SAND2009-6178
Unlimited Release
Printed September 2009

Density-Functional-Theory Results for Ga and As Vacancies in GaAs Obtained Using the Socorro Code

Alan F. Wright

Prepared by
Sandia National Laboratories
Albuquerque, New Mexico 87185 and Livermore, California 94550

Sandia is a multiprogram laboratory operated by Sandia Corporation,
a Lockheed Martin Company, for the United States Department of Energy's
National Nuclear Security Administration under Contract DE-AC04-94AL85000.

Issued by Sandia National Laboratories, operated for the United States Department of Energy by Sandia Corporation.

Available to DOE and DOE contractors from
U.S. Department of Energy
Office of Scientific and Technical Information
P.O. Box 62
Oak Ridge, TN 37831

Telephone: (865) 576-8401
Facsimile: (865) 576-5728
E-Mail: reports@adonis.osti.gov
Online ordering: http://www.osti.gov/bridge

Available to the public from
U.S. Department of Commerce
National Technical Information Service
5285 Port Royal Rd.
Springfield, VA 22161

Telephone: (800) 553-6847
Facsimile: (703) 605-6900
E-Mail: orders@ntis.fedworld.gov
Online order: http://www.ntis.gov/help/ordermethods.asp?loc=7-4-0#online

SAND2009-6178
Unlimited Release
Printed September 2009

Density-Functional-Theory Results for Ga and As Vacancies in GaAs Obtained Using the Socorro Code

Alan F. Wright
Physical, Chemical, and Nano Sciences Center
Sandia National Laboratories
P.O. Box 5800
Albuquerque, NM 87185-1415

Abstract

The Socorro code has been used to obtain density-functional theory results for the Ga vacancy (V_{Ga}) and the As vacancy (V_{As}) in GaAs. Calculations were performed in a nominal 216-atom simulation cell using the local-density approximation for exchange and correlation. The results from these calculations include: 1) the charge states, the atomic configurations of stable and metastable states, 3) energy levels in the gap, and 4) activation energies for migration. Seven charge states were found for the Ga vacancy (-3, -2, -1, 0, +1, +2, +3). The stable structures of the -3, -2, -1, and 0 charge states consist of an empty Ga site with four As neighbors displaying T_d symmetry. The stable structures of the +1, +2, and +3 charge states consist of an As antisite next to an As vacancy; As_{Ga}-V_{As}. Five charge states were found for the As vacancy (-3, -2, -1, 0, +1). The stable structures of the -1, 0, and +1 charge states consist of an empty As site with four Ga neighbors displaying C_{2v} symmetry. The stable structures of the -3 and -2 charge states consist of a Ga antisite next to a Ga vacancy; Ga_{As}-V_{Ga}. The energy levels of V_{Ga} lie below mid-gap while the energy levels of As_{Ga}-V_{As} lie above and below mid-gap. All but one of the V_{As} energy levels lie above mid-gap while the As_{Ga}-V_{As} energy level lies below mid-gap. The migration activation energies of the defect states were all found to be larger than 1.35 eV.

Acknowledgments

A. F. Wright acknowledges helpful discussions with N. A. Modine on various aspects of this research and the use of his computer code for computing a maximum likelihood fit of the As_{Ga} formation energies. Sandia is a multiprogram laboratory operated by Sandia Corporation, a Lockheed Martin Company, for the United States Department of Energy's National Nuclear Security Administration under Contract DE-AC04-94AL85000.

Contents

Introduction:

This report documents density-functional-theory (DFT) calculations performed as part of the QASPR (Qualification Alternatives to the Sandia Pulsed Reactor) program for the Ga vacancy (V_{Ga}) and As vacancy (V_{As}) in GaAs. The results obtained from these calculations include: 1) the charge states, 2) the atomic configurations and symmetry groups of stable and metastable states, 3) energy levels in the gap, and 4) activation energies for migration. In the initial planning for these calculations, it was decided to employ a moderate level of rigor in order to obtain results quickly that could be used to define a first-order model of defect physics in GaAs-based electronic devices. As such, the activation energies and energy levels should be viewed as preliminary because they are not yet converged with respect to the number of sampling points in the Brillouin zone and the size of the simulation cell (supercell). The remainder of this report is organized as follows: Section I describes the procedures employed in the calculations. This Section and also Section III are written for an audience familiar with DFT terminology. Section II presents the results and provides guidance as to effects due to the lack of convergence noted above. Section III outlines additional calculations that will be needed to obtain fully converged results. The Appendix documents auxiliary DFT calculations performed for the As antisite (As_{Ga}) in GaAs. In contrast to the results for V_{Ga} and V_{As}, the As_{Ga} results are converged with respect to Brillouin zone sampling and the size of the supercell. There are two reasons to present these results. First, in DFT calculations of energy levels it is necessary to obtain an energy shift to align the computed and measured valence-band edge (VBE) energies. This shift was obtained by comparing the lower of the two measured energy levels of As_{Ga} and the corresponding computed level. Second, an estimate of the accuracy of the computed energy levels of V_{Ga} and V_{As} can be made by comparing the difference in the two measured energy levels and the corresponding difference in the corresponding two computed energy levels. Finally, it is worthwhile noting that while there are experimental results for V_{As}, we do not attempt to compare with these results here due to the lack of convergence noted above. Background information on experimental studies and previous theoretical studies can be found in the SAND report (SAND-2009-4949J) entitled “Simple intrinsic defects in gallium arsenide” written by Sandia author P. A. Schultz along with corresponding results obtained using the SeqQUEST code.

I: Procedures

DFT calculations for V_{Ga} and V_{As} were performed using the Socorro code [1] with a plane wave basis and norm-conserving pseudopotentials (NCP’s). The Local-Density Approximation (LDA) for exchange and correlation was used in these calculations with the Perdew-Wang formulation of LDA correlation. Hamann-type Ga and As NCP’s were constructed using the fhi98PP code from the Fritz-Haber Institute. [2] Three valence electrons were treated explicitly in the Ga NCP’s and five were treated explicitly in the As NCP’s. In both the Ga and As NCP’s non-linear core corrections were employed and the *s* potentials were used as the local potentials. Furthermore, for use in the Socorro code, the semi-local pseudopotentials obtained from the the fhi98PP code were converted

into Kleinman-Bylander non-local forms using the convert.f90 code written by the author. The input files used to construct the Ga and As NCP's are given below.

```
31.00  6  2  8  1.20 : z  nc  nv iexc rnlc
   1  0   2.00      : n  l   f
   2  0   2.00
   2  1   6.00
   3  0   2.00
   3  1   6.00
   3  2  10.00
   4  0   2.00
   4  1   1.00
2  h              : lmax  s_pp_def
0  1.10  0.00  h     : lt  rct  et  s_pp_type
1  1.30  0.00  h
2  2.25  0.00  h

33.00  6  2  8  1.00  : z ncor nval iexc rnlc
     1  0    2.00   : n l occ
     2  0    2.00
     2  1    6.00
     3  0    2.00
     3  1    6.00
     3  2   10.00
     4  0    2.00
     4  1    3.00
2  h               : lmax type
0 1.00 0.0 h
2 1.80 0.0 h
```

To test the Ga and As NCP's, they were used to obtain the equilibrium lattice constant and bulk modulus of GaAs as a function of the energy cutoff defining the size of the plane wave basis used to expand the DFT Kohn-Sham wavefunctions. The results are listed in Table I below:

Table I: Predicted lattice constant and bulk modulus of GaAs for various values of the energy cutoff defining the size of the plane wave basis.

energy cutoff (Ryd)	lattice constant (Bohr)	bulk modulus (Mbar)
25	10.6184	0.760
30	10.5897	0.721
35	10.5949	0.719
40	10.5919	0.721

Based on these results, an energy cutoff of 30 Ryd was chosen for use in the V_{Ga}, V_{As}, and As_{Ga} calculations. It should be noted that the predicted lattice constant at the 30 Ryd cutoff energy is 0.84% smaller than the measured value (10.68 Bohr) and the predicted bulk modulus is 4.6% smaller than the measured value (0.756 Mbar). This level of agreement is typical for DFT calculations using the LDA. Also typical of DFT-LDA calculations, the predicted band gap (0.73 eV) is much smaller than the measured value (1.52 eV).

The DFT calculations for V_{Ga} and V_{As} were performed in a 216-atom simple cubic supercell using a maximum of 27 points to sample the Brillouin zone (corresponding to {3,3,3} Monkhorst-Pack parameters). A 216-atom supercell of bulk GaAs was first constructed using a 10.59 Bohr lattice constant. DFT calculations were performed in this bulk supercell using {2,2,2} and {3,3,3} Monkhorst-Pack parameters in order to obtain quantities needed to analyze results from the defect calculations. These quantities were the energy per GaAs unit; the eigenvalue corresponding to the VBE energy; and the decomposition of the eigenstates into *s*, *p*, and *d* components.

Local-energy minimum structures of V_{Ga} (V_{As}) were identified using the following procedure: 1) a Ga (As) atom was removed from the bulk supercell to produce an unrelaxed vacancy, 2) the positions of the four As (Ga) atoms surrounding the vacancy were shifted by small distances (≤ 0.5 Bohr) to produce a structure with no symmetries, and 3) the structure was relaxed using the quench minimization algorithm in the Socorro code. Once the structure was relaxed, the check_symmetry code in the Socorro package was used to detect symmetries in the relaxed configuration. If symmetries were detected, the structure was symmetrized to machine precision and relaxed further to verify that the structure indeed was a local-energy minimum. This process was performed for charge states ranging from -3 to +3. It is noted that these initial calculations were performed using {2,2,2} Monkhorst-Pack parameters (maximum of 8 sampling points). After local-energy minimum structures were identified, these structures were refined further using {3,3,3} Monkhorst-Pack parameters. To verify that this set of charge states was sufficient and to determine the legitimate charge states of V_{Ga} (V_{As}), the eigenstates were then decomposed and compared with the bulk supercell decompositions noted above.

An additional starting structure for V_{Ga} (V_{As}) was generated by shifting one of the surrounding four As (Ga) atoms to the vacant site in the unrelaxed vacancy structure, thereby producing an unrelaxed antisite-vacancy complex; As_{Ga}-V_{As} (Ga_{As}-V_{Ga}). As in the procedure described above, the positions of the atoms near this complex were then shifted by small distances to produce no symmetries, the structure was relaxed using the Socorro quench minimization algorithm (using {2,2,2} Monkhorst-Pack parameters), symmetries were detected using the check_symmetry code, and structures having symmetry were symmetrized to machine precision and relaxed further to verify that they were indeed local-energy minima. This was repeated for charge states ranging from -3 to +3, the local-energy minimum structures were then refined using {3,3,3} Monkhorst-Pack parameters, and the sufficiency of this set of charge states was verified by comparing decompositions of the eigenstates from the defect supercell with corresponding results from the bulk supercell.

Once the charge states and local-energy minima structures were identified, formation energies at the valence-band edge (VBE) were computed using the expression

$$E^f\left[D^q\right] = E_T\left[D^q\right] - \left(N_{GaAs} - 1\right)\mu_{GaAs} + q\left(\varepsilon_{VBE} + \Delta_{VBE}\right) \quad (1)$$

where E^f is the formation energy, E_T is the total energy from the Socorro calculation, N_{GaAs} is the number of GaAs units in the defect supercell, μ_{GaAs} is the energy per GaAs unit from the bulk calculation, ε_{VBE} is the eigenvalue at the VBE from the bulk calculation, and Δ_{VBE} is the energy shift needed to align the computed VBE energy with the measured value. As discussed in Appendix A, the value of Δ_{VBE} for GaAs is -0.409 eV. It should be noted that the complete form of Eq. 1 has an additional term: $-\mu_{As}$ (the chemical potential of an As atom) on the right hand side for V_{Ga} and As_{Ga}-V_{As} and $-\mu_{Ga}$ (the chemical potential of a Ga atom) on the right hand side for V_{As} and Ga_{As}-V_{Ga}. Since the QASPR program only requires the differences in formation energies for charge states differing by ±1 (these are the energy levels) these chemical potentials have been set to 0.

Migration paths and activation energies for V_{Ga}, As_{Ga}-V_{As}, V_{As}, and Ga_{As}-V_{Ga} were obtained using the climbing-image nudged elastic-band method (CI-NEB) with five images (not counting the stable or metastable structures used as the end points) and eight sampling points in the Brillouin zone for each image ({2,2,2} Monkhorst-Pack parameters). The end points used for the initial CI-NEB calculations were V_{Ga} (V_{As}). The rationale for this choice was based on an examination of the atomic structure near V_{Ga} and As_{Ga}-V_{As} (V_{As} and Ga_{As}-V_{Ga}), which indicated that the simplest migration paths starting or ending at As_{Ga}-V_{As} (Ga_{As}-V_{Ga}) would pass through V_{Ga} (V_{As}) and that more complicated paths would, at least temporarily, involve formation of more complicated defects.

II: Results

A: V_{Ga} and As_{Ga}-V_{As}

The charge states, formation energies, and energy levels of V_{Ga} and As_{Ga}-V_{As} are listed in Tables II and III below. (To distinguish the stable and metastable states more easily, 500 eV has been added to the formation energies.) The V_{Ga} states were all found to have T_d symmetry while the As_{Ga}-V_{As} states all have C_{3v} symmetry (the largest possible symmetry groups for these defects). The charge states of V_{Ga} are predicted to be -3, -2, -1, 0, +1, +2, +3 and the charge states of As_{Ga}-V_{As} are predicted to be 0, +1, +2, +3. The -3, -2, -1, and 0 charge states of V_{Ga} are stable while the +1, +2, and +3 charge states are metastable, i.e., they have higher energies than the corresponding charge states of As_{Ga}-V_{As}, and an energy barrier preventing them from relaxing to the stable As_{Ga}-V_{As} structure. The +1, +2, and +3 charge states of As_{Ga}-V_{As} are stable while the 0 state is metastable with respect to the V_{Ga} structure. In the -3, -2, and -1 charge states, As_{Ga}-V_{As} relaxes to the V_{Ga} structure without a barrier. The energy levels of V_{Ga} are predicted to be low in the gap while the As_{Ga}-V_{As} levels are predicted to be in both upper and lower regions of the gap. It should be kept in mind that the levels from these calculations are not converged (for reasons discussed in the introduction). At the end of this section, guidance will be given as to how large the convergence errors might be for the energy levels and for migration activation energies reported below. The atomic configurations of V_{Ga} and As_{Ga}-V_{As} are shown below (Fig. 1) in the neutral charge states. Full details of these and all other defect structures are available from the author.

Table II: Formation energies of V_{Ga} and As_{Ga}-V_{As} in eV computed using Eq. 1 (plus 500 eV).

q	-3	-2	-1	0	+1	+2	+3
$E^f[V_{Ga}]$	3.555	3.067	2.652	2.300	2.039	1.834	1.675
$E^f[As_{Ga}\text{-}V_{As}]$	unstable	unstable	unstable	2.887	1.881	1.610	0.881

Table III: Energy levels of V_{Ga} and As_{Ga}-V_{As} in eV.

level	$3^-/2^-$	$2^-/1^-$	$1^-/0$	$0/1^+$	$1^+/2^+$	$2^+/3^+$
V_{Ga}	0.488	0.415	0.352	0.261	0.205	0.159
As_{Ga}-V_{As}	NA	NA	NA	1.006	0.280	0.729

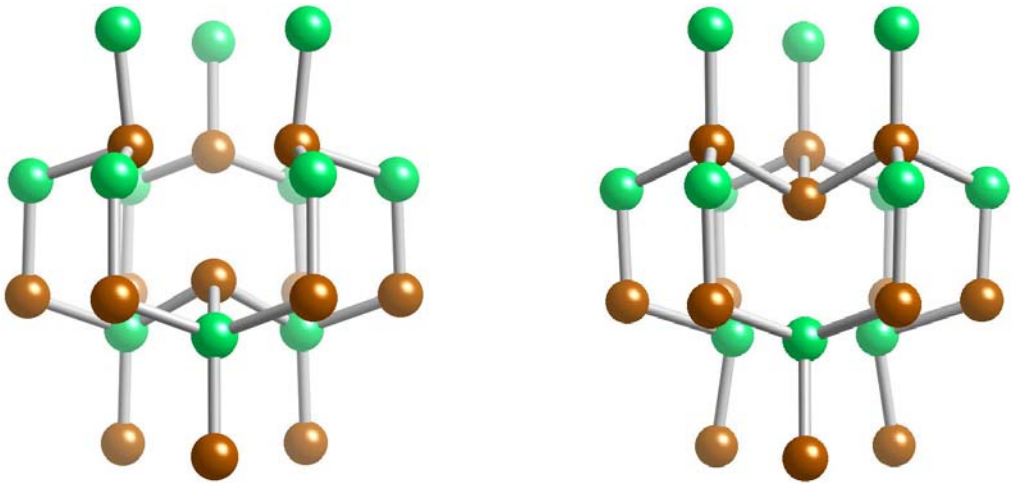

Figure 1: Atomic configurations of V_{Ga} (left) and As_{Ga}-V_{As} (right). Green spheres represent Ga and brown spheres represent As. The view is orthographic and the [111] direction is vertical. The transformation between V_{Ga} and As_{Ga}-V_{As} involves movement of an As along the [111]] direction.

The predicted activation energies (E_A) for migration of V_{Ga} and As_{Ga}-V_{As} are listed in Table IV below. As noted in Section I, the CI-NEB calculations were performed using V_{Ga} end points for the migration path. In the -3, -2, -1, and 0 charge states for which V_{Ga} is the stable state, the activation energy is computed as the difference in the formation energy at the saddle point and the formation energy of the V_{Ga} stable state. In the +1, +2, and +3 charge states for which V_{Ga} is metastable and As_{Ga}-V_{As} is the stable state, the activation energy is computed as the difference in the formation energy at the saddle point and the formation energy of the As_{Ga}-V_{As} stable state. (Note that this assumes that the energy barrier to transform from As_{Ga}-V_{As} to V_{Ga} is smaller than the barriers listed below for the +1, +2, and +3 charge states.) Since the temperature of interest to the QASPR program is room temperature and these energies are large relative to kT at room temperature (0.026 eV), these results indicate that it is unlikely that V_{Ga} or As_{Ga}-V_{As} will move a significant distance at room temperature. The atomic configurations of V_{Ga} during migration are shown below (Fig. 2) in the neutral charge state.

Table IV: Activation energies for V_{Ga} and As_{Ga}-V_{As} migration in eV.

q	-3	-2	-1	0	+1	+2	+3
E_A	1.843	1.595	1.351	1.475	1.592	1.637	2.140

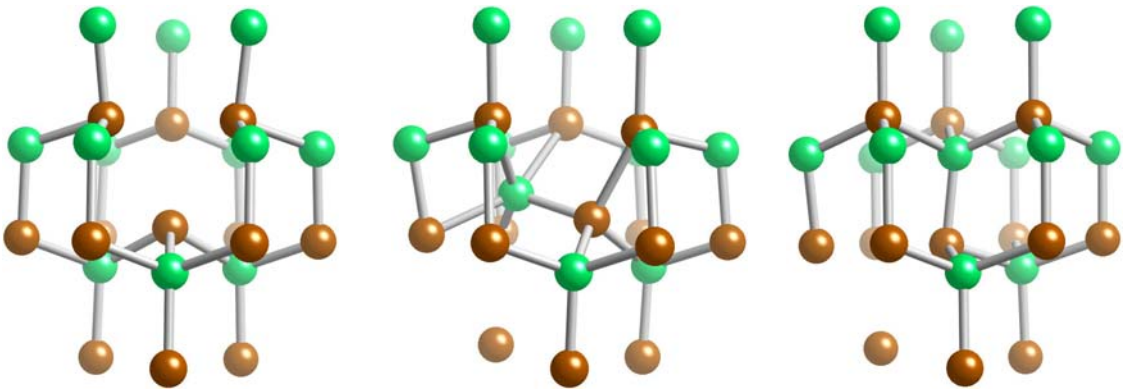

Figure 2: Atomic configurations of V_{Ga} during migration: initial stable state (left), saddle point (middle), final stable state (right). Green spheres represent Ga and brown spheres represent As. The view is orthographic and the [111] direction is vertical.

B: V_{As} and Ga_{As}-V_{Ga}

The charge states, formation energies, and energy levels of V_{As} and Ga_{As}-V_{Ga} are listed in Tables V and VI below. (To distinguish the stable and metastable states more easily, 277 eV has been added to the formation energies.) The V_{As} states were all found to have C_{2v} symmetry while the Ga_{As}-V_{Ga} states were found to have C_{3v} symmetry. C_{3v} is the largest possible symmetry group for Ga_{As}-V_{Ga}, but C_{2v} is not the largest possible symmetry group for V_{As} reflecting an energy lowering rearrangement of the surrounding four Ga atoms. The charge states of V_{As} are predicted to be -3, -2, -1, 0, +1 and the charge states of Ga_{As}-V_{Ga} are predicted to be -3, -2. The -1, 0, and +1 charge states of V_{As} are stable while the -3 and -2 charge states are metastable, i.e., they have higher energies than the corresponding charge states of Ga_{As}-V_{Ga} and an energy barrier preventing them from relaxing to the stable Ga_{As}-V_{Ga} structure. The -3 and -2 charge states of Ga_{As}-V_{Ga} are stable. In the -1, 0, and +1 charge states, Ga_{As}-V_{Ga} relaxes to the V_{As} structure without a barrier. The energy levels of V_{As} are predicted to be high in the gap except for the $1^-/0$ level which is predicted to lie below mid-gap. The Ga_{As}-V_{Ga} level is predicted to be below mid-gap, slightly above the V_{As} $1^-/0$ level. As noted above, it should be kept in mind that the levels from these calculations are not yet converged (for reasons discussed in the introduction). The atomic configurations of V_{As} and Ga_{As}-V_{Ga} are shown below (Fig. 3) in the neutral and -2 charge states, respectively.

Table V: Formation energies of V_{As} and Ga_{As}-V_{Ga} in eV computed using Eq. 1 (plus 277 eV).

q	-3	-2	-1	0	+1
$E^f[V_{As}]$	4.823	3.634	2.416	1.904	0.941
$E^f[Ga_{As}$-$V_{Ga}]$	4.144	3.561	unstable	unstable	unstable

Table VI: Energy levels of V_{As} and Ga_{As}-V_{Ga} in eV.

level	$3^-/2^-$	$2^-/1^-$	$1^-/0$	$0/1^+$
V_{As}	1.189	1.218	0.512	0.963
Ga_{As}-V_{Ga}	0.583	NA	NA	NA

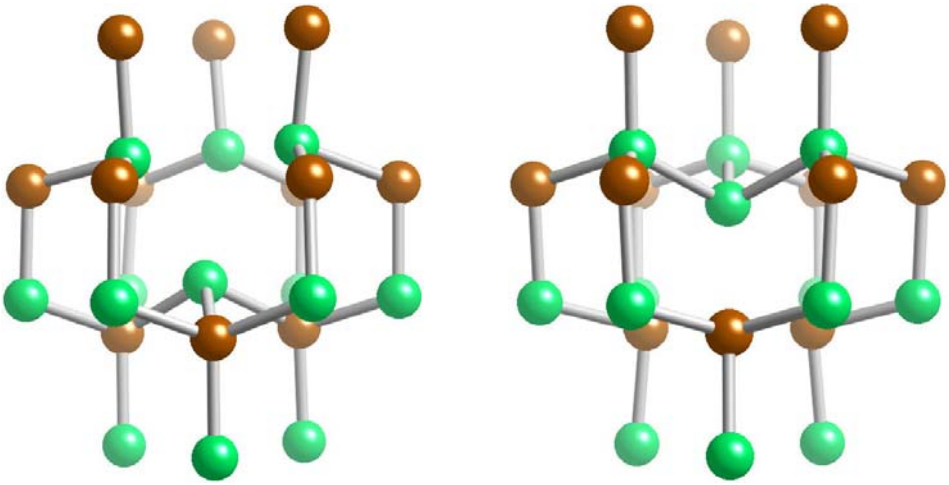

Figure 3: Atomic configurations of V_{As} (left) and Ga_{As}-V_{Ga} (right). Green spheres represent Ga and brown spheres represent As. The view is orthographic and the [111] direction is vertical. The transformation between V_{As} and Ga_{As}-V_{Ga} involves movement of a Ga along the [111]] direction.

The predicted activation energies (E_A) for migration of V_{As} and Ga_{As}-V_{Ga} are listed in Table VII below. As noted in Section I, the CI-NEB calculations were performed using V_{As} end points for the migration path. In the -1, 0, and +1 charge states for which V_{As} is the stable state, the activation energy is the difference in the formation energy at the saddle point and the formation energy of the V_{As} stable state. In the -3 and -2 charge states for which V_{As} is metastable and Ga_{As}-V_{Ga} is the stable state, the activation energy is computed as the difference in the formation energy at the saddle point and formation energy of the Ga_{As}-V_{Ga} stable state. (This assumes that the energy barrier to transform from Ga_{As}-V_{Ga} to V_{As} is smaller than the barriers listed below for the -3 and -2 charge states.) Since the temperature of interest to the QASPR program is room temperature and these energies are large relative to kT at room temperature (0.026 eV), these results indicate that it is unlikely that V_{As} or Ga_{As}-V_{Ga} will move a significant distance at room temperature. The atomic configurations of V_{As} during migration are shown below (Fig. 4) in the neutral charge state.

Table IV: Activation energies for V_{As} and Ga_{As}-V_{Ga} migration in eV.

q	-3	-2	-1	0	+1
E_A	2.137	1.816	1.981	2.016	2.046

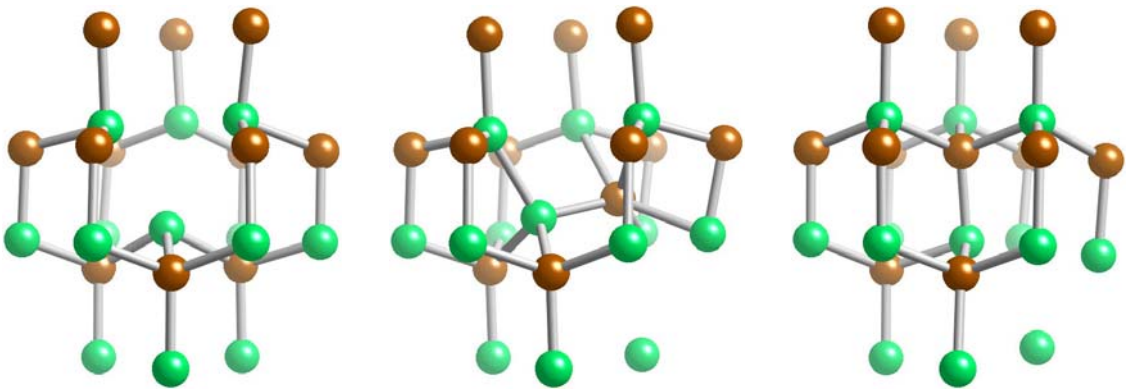

Figure 4: Atomic configurations of V_{As} during migration: initial stable state (left), saddle point (middle), final stable state (right). Green spheres represent Ga and brown spheres represent As. The view is orthographic and the [111] direction is vertical.

C: Effects due to the lack of convergence

Estimates of the effects due to the lack of convergence in these results can be obtained by examining previous calculations [3] for the silicon vacancy (V_{Si}) that *were* converged with respect to the number of Brillouin zone sampling points and the size of the supercell. The V_{Si} calculations used nominal 216-, 512-, and 1000-atom supercells, the LDA, and {5,5,5}, {4,4,4}, and {3,3,3} Monkhorst-Pack parameters, respectively, to specify sampling points in the Brillouin zone. The formation energies obtained from these three supercells were then extrapolated to infinite supercell size using a maximum likelihood fit to the Makov-Payne formula truncated at the $1/L^3$ term. In Table V below, V_{Si} formation energies are given from these extrapolations and from calculations using a 216-atom supercell and {3,3,3} Monkhorst-Pack sampling of the Brillouin zone (the procedure used in this study). The results in Table V indicate that significant deviations from converged formation energies occur for all charge states, but are largest for negative charge states and increase with the magnitude of the charge state. In Table VI, V_{Si} energy levels obtained from these two sets of formation energies are given. Likewise, the deviations from converged energy levels are largest for transitions involving at least one negative charge state. Corresponding comparisons of V_{Si} migration activation energies are shown in Table VII. In this case, a full set of results were not available using the LDA so results are shown instead for the PBE form of the generalized gradient approximation (GGA). Also, the Brillouin zone sampling mesh used in the 216-atom supercell was specified with {5,5,5} Monkhorst-Pack parameters. The two sets of results are within 0.150 eV with largest deviation occurring for the +2 charge state. Based on these results, it is likely that the effects of the lack of convergence in the GaAs results are likely to be greatest in the formation energies and energy levels and that errors as large as 0.3 eV should be expected in the energy levels. The errors in the migration activation energies will likely be 0.150 eV. The smaller errors for migration activation energies is reasonable since they are computed from the difference in two formation energies and, to some extent, the errors in these two formation energies are likely to cancel.

Table V: Formation energies (in eV) of V_{Si} using 216-atom supercells and {3,3,3} Monkhorst-Pack sampling (A) and the extrapolation technique outlined in the text (B).

q	-2	-1	0	+1	+2

A: not converged	4.635	4.133	3.529	3.296	3.004
B: converged	5.023	4.302	3.457	3.220	3.090

Table VI: Energy levels (in eV) of V_{Si} using 216-atom supercells and {3,3,3} Monkhorst-Pack sampling (A) and the extrapolation technique outlined in the text (B).

level	$2^-/1^-$	$1^-/0$	$0/1^+$	$1^+/2^+$
A: not converged	0.502	0.604	0.233	0.292
B: converged	0.721	0.845	0.237	0.130

Table VII: Migration activation energies (in eV) of V_{Si} using 216-atom supercells and {3,3,3} Monkhorst-Pack sampling (A) and the extrapolation technique outlined in the text (B).

q	-2	-1	0	+1	+2
A: not converged	0.135	0.044	0.262	0.223	0.405
B: converged	0.151	0.035	0.355	0.190	0.273

III: Additional calculations needed to obtain converged results

There are three aspects to obtaining converged results. The first concerns the technical aspects of sampling in the Brillouin zone and the supercell size dependence of results for mainly charged defects but also neutral defects. Based on results obtained previously for defects in silicon and on results obtained for As_{Ga} in GaAs (and discussed in Appendix A), it is recommended that additional calculations be performed using nominal 512- and 1000-atom supercells with Monkhorst-Pack parameters {4,4,4} and {3,3,3}, respectively, used to generate sampling points in the Brillouin zone. Additional calculations should also be performed in the 216-atom supercell to extend the Brillouin zone sampling to that obtained with Monkhorst-Pack parameters {5,5,5}. The second aspect concerns the choice of which Ga electrons to treat explicitly. It is not yet established whether or not the present treatment of three electrons is adequate and, at the very least, tests should be performed to evaluate whether or not it will be necessary to instead treat 13 electrons explicitly. These tests would require using the projector-augmented wave (PAW) method instead of the NCP method, but the expectation is that doing so will also permit use of a smaller cutoff to define the plane wave basis. The third aspect concerns the formulation of the exchange and correlation functional. Results for defects in silicon clearly indicated that the PBE form of the GGA was superior to the LDA in that the PBE results correctly reproduced the negative-U behavior of V_{Si} whereas the LDA did not. It is recommended that tests be performed to evaluate the differences between LDA and PBE results before deciding which formulation to use for in calculations using the 512- and 1000-atom supercells.

References

1. See http://dft.sandia.gov/socorro.

2. See http://www.fhi-berlin.mpg.de/th/fhi98PP/.

3. A. F. Wright, Phys. Rev. B **74**, 165116 (2006).

4. J. Lagowski, D. G. Lin, T. –P. Chen, M. Skonwronski, and H. C. Gates, Appl. Phys. Lett. **47**, 929 (1985).

Appendix

As noted in the Introduction, DFT calculations were performed for As_{Ga} in order to: 1) obtain the energy shift (Δ_{VBE}) needed to align the computed and measured energy levels and 2) obtain an estimate of the accuracy of DFT for defects in GaAs. As_{Ga} calculations were performed for -1, 0, +1, and +2 charge states using the procedures described in Section I to identify the charge states and local-energy minimum structures. However, in contrast to the procedures described in Section I the As_{Ga} calculations were performed in nominal 216-, 512-, and 1000-atom supercells using {5,5,5}, {4,4,4}, and {3,3,3} Monkhorst-Pack parameters, respectively, to generate sampling points in the Brillouin zone. As_{Ga} formation energies (with Δ_{VBE} temporarily set to zero) were computed using the three supercells and the values were then extrapolated to infinite cell size using a maximum likelihood fit to the Makov-Payne equation, truncated at the $1/L^3$ term where L is the length of one side of the supercell, and a static dielectric constant of 12.0. The charge states were found to be 0, +1, and +2 and the local-energy minimum structures all were found to have the T_d symmetry group. The extrapolated formation energies (with 225 eV added and Δ_{VBE} set to 0) are listed in Table A1 below. The energy levels obtained from these formation energies are listed in Table A2.

Table A1: Formation energies (in eV with 225 eV added) of As_{Ga} computed using Eq. 1 with Δ_{VBE} set to 0.

q	0	+1	+2
$E^f[As_{Ga}]$	4.615	4.249	4.118

Table A2: Energy levels (in eV) of As_{Ga} with Δ_{VBE} set to 0.

level	$0/1^+$	$1^+/2^+$
As_{Ga}	0.366	0.131

Two energy levels have been observed [4] for the EL2 center in *p*-type GaAs, which is believed to be As_{Ga}. The lower level ($1^+/2^+$) lies 0.54 eV above the VBE and the upper level ($0/1^+$) lies 0.75 eV below the conduction-band edge or 0.23 eV above the lower level, assuming that the band gap of GaAs is 1.52 eV. Comparison of the measured and computed $1^+/2^+$ levels indicates that Δ_{VBE} = -0.409 will bring them into agreement. With regard to the general accuracy of DFT defect energy levels in GaAs, it is noted that the computed levels are separated by 0.235 eV, which is only 0.005 eV larger than the measured separation. This is rather good agreement but some words of caution are needed. For cases where comparisons can be made, computed energy levels of donor defects in silicon that lie in the lower half of the gap are generally in good agreement with measurements while the agreement is poorer for energy levels of acceptor defects in the upper half of the gap. One reason for this discrepancy is the tendency of DFT to spread out defect charge distributions of acceptor defects because (correctly) having a more compact distribution increases the total energy due to unphysical electron self-interactions present in LDA and GGA exchange-correlation functionals.

DISTRIBUTION:

1	MS 0899	Technical Library, 9536 (electronic copy)
1	MS 1415	Diane Peebles, 01112
2	MS 1415	Sam Myers, Jr., 1110